arXiv:1711.06686v1 [cond-mat.supr-con] 17 Nov 2017

Ubiquitous Spin-Orbit Coupling in Iron-Based Superconductors

R.P. Day[1,2], G. Levy[1,2], M. Michiardi[1,2], M. Zonno[1,2], F. Ji[1,2], E. Razzoli[1,2], F. Boschini[1,2], S. Chi[1,2], R. Liang[1,2], P.K. Das[3,4], I. Vobornik[3], J. Fujii[3], D.A. Bonn[1,2], W.N. Hardy [1,2], I.S. Elfimov[1,2], A. Damascelli[1,2*]

[1]*Department of Physics and Astronomy, University of British Columbia, Vancouver, BC V6T 1Z1, Canada*

[2]*Quantum Matter Institute, University of British Columbia, Vancouver, BC V6T 1Z4, Canada*

[3]*Istituto Officina dei Materiali (IOM)-CNR, Laboratorio TASC, Area Science Park, S.S.14, Km 163.5, I-34149 Trieste, Italy*

[4]*International Centre for Theoretical Physics (ICTP), Strada Costiera 11, I-34100 Trieste, Italy*

The iron-based superconductors (FeSCs) reside in a rich region of phase space, where small modifications to structure and stoichiometry have the capacity to shift the electronic ground state between phases as varied as magnetic ordering and multiband superconductivity[1–4]. The proximity of several shallow Fermi surface pockets render these materials highly susceptible to the influence of correlations, nematicity, and the atomic effects of spin-orbit coupling (SOC). By employing Circularly Polarized Spin and Angle-Resolved Photoemission Spectroscopy (CPS-ARPES) to study archetypal members of both Fe-pnictides and Fe-chalcogenides, we demonstrate here evidence for ubiquitous coupling of spin and orbital

*damascelli@phas.ubc.ca

degrees of freedom in the FeSCs. This result has fundamental implications for Fe-based superconductivity as the loss of independence in these degrees of freedom introduces spin triplet terms to the putative singlet pairing symmetry, and mandates consideration of a momentum-dependent binding of spin and orbital degrees of freedom in the study of possible pairing mechanisms.

In order to establish the fundamental criteria for superconductivity in the FeSCs, there is considerable debate at present as to the significance and ubiquity of various interactions in these materials[1]. To this end, the effects of Coulomb's and Hunds' coupling, as well as nematic ordering have been of primary focus. Furthermore, as SOC has been put forth to explain deviations in ARPES from the non-relativistic band structure, there is much interest now in the extent to which this interaction influences the electronic eigenstates relevant to superconductivity[5,6]. To attribute definitively the gaps observed in ARPES to SOC, explicit evidence of a coupling of the nominative spin and orbital degrees of freedom is necessary. At the Brillouin zone centre for example, other perturbations such as nematicity can lead to nearly indistinguishable changes to the electronic dispersion from those induced by SOC[7]. CPS-ARPES is an experimental technique capable of making this distinction, providing evidence that the spin-orbit interaction binds these degrees of freedom in a strongly momentum-dependent way, predominantly affecting the hole pockets near the zone centre (i.e. the $\overline{\Gamma Z}$ direction where $k_{||} = 0$ $\mathring{A}^{-1}$).

While ARPES is defined broadly as a probe of the one electron-removal spectral function, the photocurrent is modulated by dipole matrix element effects which encode information regarding

both the experimental configuration such as light polarization as well as the nature of the wave-function being probed[8,9]. In CPS-ARPES, circularly polarized light photoemits preferentially from states of specific angular momentum m_l, and by spin-filtering the resulting photocurrent one can measure directly the correlation between the spin and orbital degrees of freedom[10–12]. With the aim then of exploring the relationship between $\vec{L}$ and $\vec{S}$ in the FeSCs, we report here on the study of archetypal members of the Fe-pnictides (LiFeAs) and Fe-chalcogenides (FeSe) via CPS-ARPES.

To illustrate the application of this technique to the FeSCs, we begin by considering the two hole pockets common to all FeSCs near the Brillouin zone center. Each band is doubly degenerate and composed primarily of Fe d_{xz} and d_{yz} orbitals. In the presence of SOC, the four-fold degeneracy at zone centre ($k_{||} = 0$ $\mathring{A}^{-1}$) is split and two Kramers' doublets split by 10 - 20 meV remain (Figure (1a)): one doublet defined with the $\hat{\mathbf{z}}$ projection of the orbital and spin angular momentum aligned parallel ($d^{\uparrow z}_{+1z} = Y_{21}\,|+\chi\rangle$ and $d^{\downarrow z}_{-1z} = Y_{2,-1}\,|-\chi\rangle$) and the other doublet antiparallel ($d^{\uparrow z}_{-1z} = Y_{2,-1}\,|+\chi\rangle$ and $d^{\downarrow z}_{+1z} = Y_{2,1}\,|-\chi\rangle$). These pairs are illustrated for the case of LiFeAs in Figure (1). Here we have used the basis of the direct product space over spherical harmonics $Y_{l,m}(\theta,\phi)$ and spin-$\frac{1}{2}$ spinors $|\pm\chi\rangle$ with the quantization axis $\hat{\mathbf{z}}$ defined out of the Fe-pnictogen/chalcogen plane.

Under the dipole approximation $\Delta l = \pm 1$ during photoemission, and for circularly polarized light selection rules are further restricted allowing only $\Delta m_l = 1$ for C_+, and $\Delta m_l = -1$ for C_- light. Here and throughout, the photoelectron final state is approximated by a free-electron plane wave[8]. For C_+ light as an example, photoemission from the $Y_{2,-1}$ state is dominant, and here

this would restrict photoemission from only $d^{\uparrow z}_{-1z}$ and $d^{\downarrow z}_{-1z}$[13]. Photoelectrons from these states are then spin-filtered by the VLEED detector[14]. In this way one has control over both the orbital from which photoemission occurs, and the spin which is measured. To apply this technique towards elucidating the binding of spin and orbital degrees of freedom, one measures the spin polarization asymmetry defined as[10]

$$P_i = \frac{\sqrt{I^{\uparrow}_{-} I^{\downarrow}_{+}} - \sqrt{I^{\uparrow}_{+} I^{\downarrow}_{-}}}{\sqrt{I^{\uparrow}_{-} I^{\downarrow}_{+}} + \sqrt{I^{\uparrow}_{+} I^{\downarrow}_{-}}} \tag{1}$$

where $I^{\uparrow(\downarrow)}_{+(-)}$ indicates the photocurrent intensity for C_+ (C_-) light incident on the $\uparrow(\downarrow)$ spin detector oriented along the $i = \hat{\mathbf{x}}, \hat{\mathbf{y}}, \hat{\mathbf{z}}$ direction. Under consideration of the dipole selection rules above, $I^{\uparrow}_{-} I^{\downarrow}_{+}$ is a measure of states with orbital and spin aligned parallel, and $I^{\uparrow}_{+} I^{\downarrow}_{-}$ a measure of those aligned antiparallel. Consequently, CPS-ARPES is the most direct measure of the effects of SOC, with P_i offering an energy and momentum-resolved measure of the spin-orbit coupling polarization. In the absence of SOC, where another interaction such as nematicity has induced a splitting of bands, P_i would vanish everywhere, as $C_\pm$ would photoemit from the Kramers' degenerate states of $|+\chi\rangle$ and $|-\chi\rangle$ indiscriminately. By measuring P_i throughout the Brillouin zone and along different axes of spin projection, we may study the impact of spin-orbit coupling throughout the electronic structure of the FeSCs.

Due to its relationship to SOC and the related splittings in the band structure, in Figure (1a), we follow the evolution of $\left\langle \vec{L} \cdot \vec{S} \right\rangle$ along high symmetry directions for the case of LiFeAs (see

Methods). In fitting the model to the measured dispersion, atomic SOC of strength $\lambda_{SOC} = 40$ meV has been added to the non-relativistic Hamiltonian, and the electronic band structure then renormalized by a factor of 2.19 to account for correlation effects in ARPES, as in Figure (2a). This renormalization of the spectral function is consistent with those observed throughout the FeSCs[1,4,15]. As illustrated in Figure (2c), a splitting of 13 $\pm$ 3 meV at the zone centre is extracted from a fit to energy distribution curves (EDCs), which is similar to the splitting measured elsewhere[6]. From Figure (1a), the influence of SOC is most pronounced on the hole pockets at the zone centre near E_F. We plot $\langle L_z S_z \rangle$ and $\langle L_x S_x \rangle$ in Figure (1b) and (1c) since experimentally, we measure P_i along the out of plane and $\overline{\Gamma M}$ (i.e. Fe-Fe) directions which we designate as $\hat{\mathbf{z}}$ and $\hat{\mathbf{x}}$ respectively.

Motivated by the calculations of $\left\langle \vec{L} \cdot \vec{S} \right\rangle$, experimental emphasis was placed on emission angles near $k_{||} = 0$, where we collected spin-resolved EDCs from LiFeAs with C_+ and C_- light and spin projected along both $\hat{\mathbf{z}}$ and $\hat{\mathbf{x}}$. For each emission angle we computed P_z as in Equation 1 and the result is plotted in Figure (3a). The two spectral peaks denoted in Figure (2c) can be ascribed to the $d^{\uparrow\downarrow z}_{\pm 1 z}$ and $d^{\uparrow\downarrow z}_{\mp 1 z}$ states defined earlier with spin and orbital angular momentum antiparallel at high binding energy, and parallel closer to the Fermi level. In a plot of the polarization asymmetry (Figure (3)), this is reflected by a switch in the sign of P_z between the two peaks, reflective of the switch in sign of $\langle L_z S_z \rangle$ between the two doublets. Moving to larger $k_{||}$, the switch in P_z moves with the dispersion to higher binding energies, and at large enough $k_{||}$, only the $d^{\uparrow\downarrow z}_{\pm 1 z}$ states contributes to the ARPES intensity, resulting in $P_z > 0$.

While the inherent collection inefficiency of S-ARPES limits the resolution of our experimental evaluation of P_z in both energy and momentum, simulated CPS-ARPES intensity across the entire region of momenta and energy near the zone centre not only agrees well with the measured curves, but allows for interpolation of P_z throughout this volume of the Brillouin zone. In order to do this, simulated ARPES spectra, as in Figure (2b) were generated based on the experimental configuration (See Supplementary). The full simulated P_z spectra is plotted in Figure (3c). For more direct comparison with the data, three simulated P_z curves for the $k_{||}$ values probed experimentally are reproduced in Figure (3b). From these results we infer that the spin and orbital degrees of freedom in LiFeAs are coupled primarily near the zone centre where these bands approach the Fermi level. Only for larger in plane momenta $k_{||}$ as the bands move away from E_F do the effects of SOC become sufficiently small that the Kramers' doublets reduce to the usual $|d_{xz}/d_{yz}\rangle \otimes |\pm\chi\rangle$ used to describe these bands.

In addition to the spin-projection out of plane, we measured spin along the $\overline{\Gamma M}$ direction and found that away from $k_{||} = 0$, the spin vector tilts away from (anti)parallel alignment with $\vec{L}$ for the two hole bands. The results, plotted in Figure (S3) show this small, but larger than anticipated, in-plane spin-orbit polarization P_x. This implicitly requires hybridization with orbitals beyond d_{xz} and d_{yz}, as SOC only introduces L_zS_z terms between these states. Similar measurements (both in and out of plane) on the electron pockets at the zone corner produced no observable spin-orbital polarization (Figure (S4)), suggesting the effects of SOC on the independence of $\vec{L}$ and $\vec{S}$ to be more relevant to the hole pockets at the zone centre. This has important implications for spin and orbital fluctuation pairing mechanisms which involve intra- and inter-band exchange in these channels[2]

which are evidently co-dependent in regions of k-space relevant to superconductivity. Specifically SOC has been shown to suppress the spin-susceptibility for $\vec{Q}$ connecting hole and electron pockets in FeSCs where these fluctuations are considered particularly relevant to superconductivity.[16]

Due to the conservation of energy in the photoemission process, variation of the photon energy $h\nu$ allows for exploration of the full three-dimensional Brillouin zone[17]. In consideration of Figure (1b) and (1d), the $\langle L_z S_z \rangle$ is anticipated to vary substantively along the k_z direction between Γ and Z. While at Γ the tops of the two hole bands are below E_F and characterized by parallel and antiparallel SOC projection, at Z these bands have both moved above E_F, and an additional band drops below E_F around k_z = 0.55Z. Near to Z then, we anticipate the polarization asymmetry to be dominated by states with orbital and spin angular momentum aligned antiparallel, resulting in a strictly negative P_z curve. Experimentally, we have explored the evolution of P_z across several values of k_z by varying photon energy between 26 eV and 46 eV. This range allows for us to tune k_z from Γ to Z and on towards the next Γ point. The characteristic switch of P_z is observed for k_z near Γ, and the anticipated $P_z < 0$ curves were found near $k_z = Z$. The variation of SOC along k_z demonstrates that the occupied states have co-aligned and counter-aligned spin and orbital angular momentum states for k_z near Γ evolving to a situation with the occupied states having solely counter-aligned spin and orbital vectors closer to Z.

In contrast to LiFeAs, many of the FeSCs undergo a nematic transition as temperature is reduced towards T_c. The recurrent observation of a nematic phase near T_c in many FeSCs has motivated theoretical interest in its role in Fe-based superconductivity[18]. In FeSe for example,

there is a well-known structural distortion from tetragonal to orthorhombic around 90 K[19]. We may ask if the SOC is still of importance, or if the system is dominated by the energy scales associated with orbital ordering. In order to explore this possibility, similar measurements were performed on FeSe near both the zone centre and corners, well within the orthorhombic phase at 20 K. As evidenced by the ARPES spectra in Figure (4a) and the Fermi surface in the inset of Figure (4b), it is evident that we probe primarily one orthorhombic domain[20]. Some intensity from the twin domain is however present. As seen in Figure (4b), the polarization asymmetry near zone centre for FeSe displays a close similarity to that of LiFeAs. These similarities are not restricted to $k_{||} = 0$, but over the region explored in Figure (4b). Similar to LiFeAs, a characteristic switch in the sign of P_z is observed near normal emission, with P_z becoming increasingly dominated at larger $k_{||}$ by the larger, more slowly dispersing hole band with $\vec{L}$ and $\vec{S}$ oriented parallel. The enhanced splitting between d_{xz} and d_{yz} levels imbued by the orthorhombic distortion results in a larger amplitude in the measured P_z for FeSe. At the zone corners, we measured EDCs from both the centre and edge of the X and Y electron pockets, which overlap in the measured spectra due to the twin orthorhombic domains. For these states however, the P_z displayed in Figure (4c) shows no evidence of substantive coupling. A similar null result was acquired for the in plane spin projection. Through study of orthorhombic FeSe, we have demonstrated clearly that the orbital and spin degrees of freedom are coupled by relativistic effects in a way which is not suppressed by the introduction of nematicity. Furthermore, this provides evidence that the effects of SOC are not limited to the pnictides, but rather SOC appears to be of generic importance to the low-energy electronic structure of both principal families of the FeSCs.

The complexity and variety of phenomenology exhibited in the FeSCs is unparalleled in the study of unconventional superconductors. Despite this, the intense research effort to date has uncovered a number of common threads, the constancy of which may explain the remarkable stability of multiband superconductivity against variations in structure and stoichiometry. We have demonstrated here via CPS-ARPES that one such commonality which need be accounted for in a minimal theory for iron-based superconductivity is the effect of the spin-orbit interaction. While many interactions influence the low energy electronic states, by employing CPS-ARPES we have distinguished the influence of SOC from other perturbations such as orbital ordering. In the context of unconventional superconductivity, this further distinguishes the FeSCs from the strongly correlated cuprates, and rather is suggestive of comparison with the relativistic superconducting ruthenates[10]. The FeSCs however, illustrate the possibility for supporting high temperature superconductivity in the presence of both correlations and relativistic effects.

The principal influence of SOC on the low energy electronic structure has been shown here to be the collapse of the independence of spin and orbital degrees of freedom on the hole pockets near the Brillouin zone centre. Interestingly, these hole pockets are associated in general with the largest reported superconducting gaps[6]. One consequence of SOC on any theory of superconductivity is the need to incorporate both spin singlet and triplet terms in the pairing equations[21]. These effects can be subtle, and in the case of strongly hole-doped FeSCs, this can even be shown to be necessary for attractive pairing to occur in the s-wave channel[22]. Discussions to date have primarily disregarded triplet terms and emphasized either orbital or spin-based fluctuation mechanisms supporting some type of s-wave superconductivity. However, the SOC-induced mixing of

these channels illustrated here suggests that further consideration of the pairing mechanisms put forth thus far and their possible interplay will be needed for a more complete understanding of superconductivity in the Fe-pnictides and chalcogenides.

1 Acknowledgements

We thank O. Vafek for helpful discussions on the topic. This research was undertaken thanks in part to funding from the Max Planck UBC Centre for Quantum Materials and the Canada First Research Excellence Fund, Quantum Materials and Future Technologies Program. The work at UBC was supported by the Killam, Alfred P. Sloan, and Natural Sciences and Engineering Research Council of Canada (NSERC) Steacie Memorial Fellowships (A.D.), the Alexander von Humboldt Fellowship (A.D.), the Canada Research Chairs Program (A.D.), NSERC, Canada Foundation for Innovation (CFI) and CIFAR Quantum Materials Program. E.R. acknowledges support from the Swiss National Science Foundation (SNSF) grant no. P300P2-164649. This work has been partly performed in the framework of the nanoscience foundry and fine analysis (NFFA-MIUR Italy Progetti Internazionali) facility.

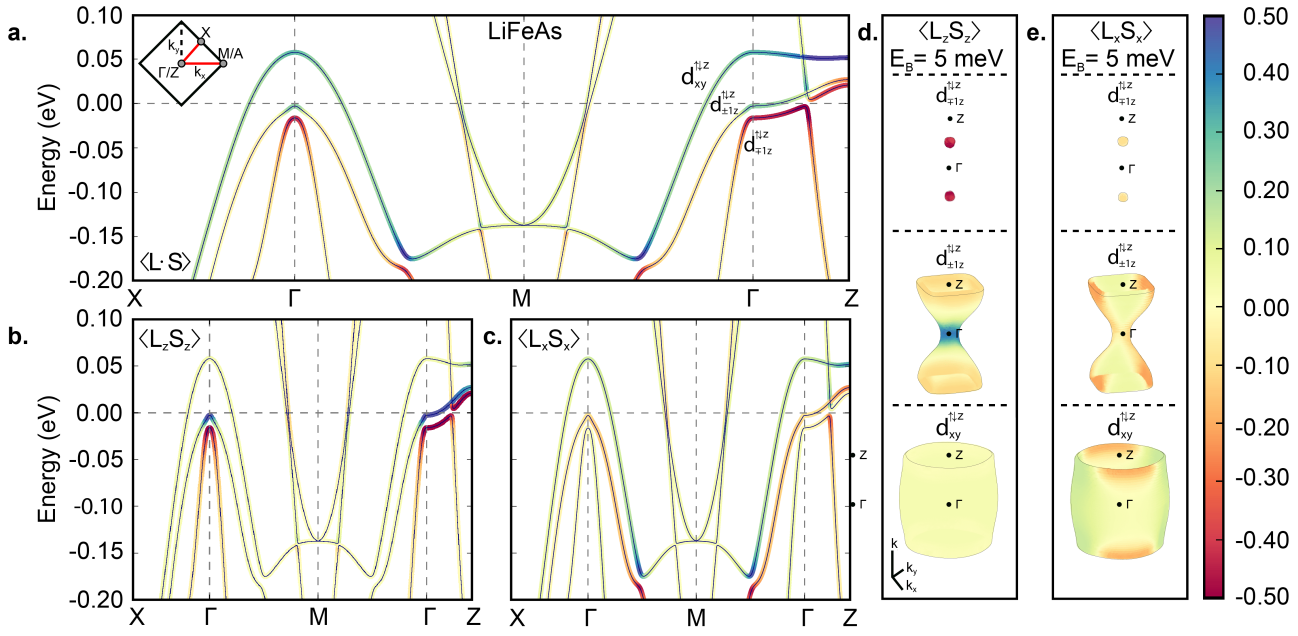

Figure 1 (a) Electronic band structure for LiFeAs with colour-scale indicating the expectation value of $\left\langle \vec{L} \cdot \vec{S} \right\rangle$ along high symmetry directions of the Brillouin zone. λ_{SOC} taken as 40 meV before renormalization. (b) Component of $\left\langle \vec{L} \cdot \vec{S} \right\rangle$ derived from the $\hat{\mathbf{z}}$ direction (i.e. along the $\overline{\Gamma Z}$ direction), and in (c), that along the $\hat{\mathbf{x}}$ direction (i.e. $\overline{\Gamma M}$). In (d) and (e), the $\langle L_z S_z \rangle$ and $\langle L_x S_x \rangle$ as in (b) and (c), but around constant energy surfaces in momentum space at an energy of $E = E_F$ - 5 meV. The $\vec{S}$ and $\vec{L}$ show largest (anti)collinear alignment near the zone centre ($\overline{\Gamma Z}$) for states near E_F on the two inner hole bands. This is directed primarily out of plane, and varies for constant energy contours along the k_z direction.

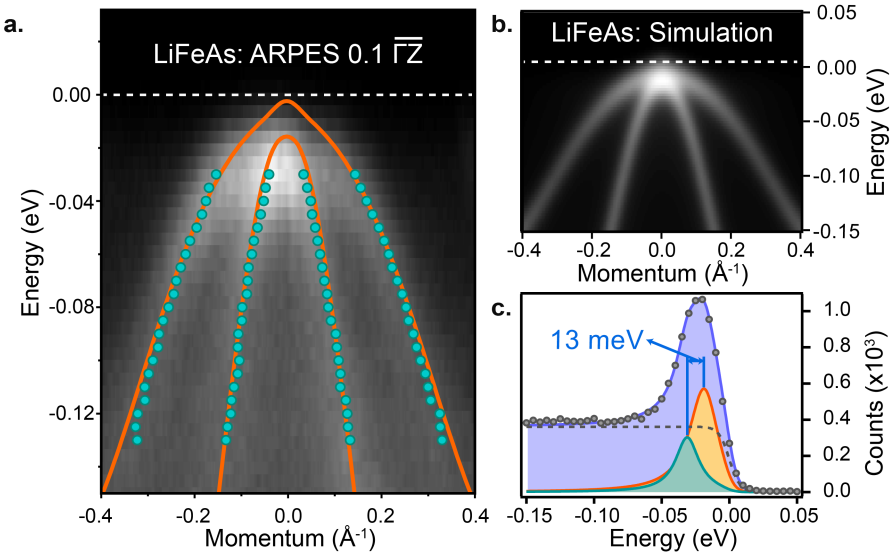

Figure 2 (a) ARPES near normal emission for LiFeAs at $h\nu = 26$ eV, corresponding to 0.1$\overline{\Gamma Z}$. Fits to MDCs are shown in blue, with the Wannier band structure underneath in orange. (b) Calculated ARPES intensity using this model at T =20 K for C_+ polarization. (c) EDC from panel (a) at $k_{||} = 0\ \AA^{-1}$, fit to the sum of background (dashed line) and two Lorentzians (blue and orange) split by 13 $\pm$ 3 meV, consistent with other reports[6]. The total fit is in purple with data points in grey.

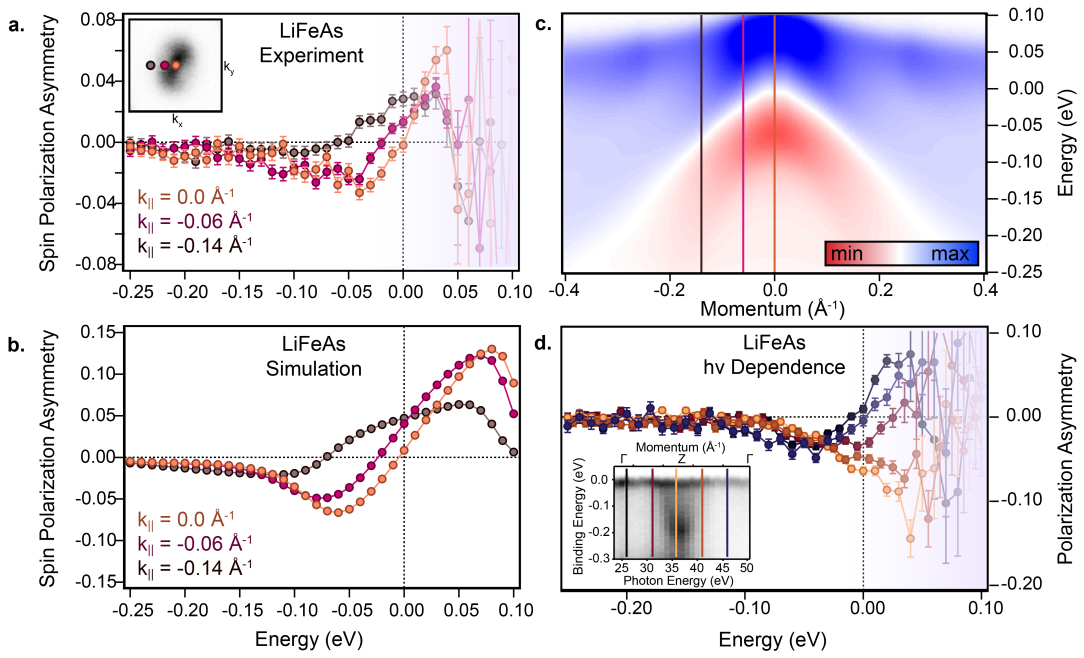

Figure 3 (a) Measurement of out of plane Spin Polarization Asymmetry at normal emission (orange), $k_{||}$ = -0.06$\mathring{A}^{-1}$ (red) and $k_{||}$ = -0.14 $\mathring{A}^{-1}$ (purple). Inset shows the Fermi surface for this region of $\vec{k}$, with symbols indicating the momenta for the three curves. (b) Calculation of P_z for the same momenta as in (a). (c) The calculated map of P_z as it varies near normal emission, vertical lines correspond to curves in (a,b). (d) Spin Polarization Asymmetry along $\overline{\Gamma Z}$. Spin polarization asymmetry was measured at $h\nu = 26$ (black), 31(red), 36(yellow), 41 (orange), and 46 (purple) eV, corresponding to $k_z = 0.1Z$, $0.5Z$, $0.9Z$, $0.7Z$, and $0.35Z$ respectively. Inset: ARPES at normal emission as a function of photon energy–vertical lines indicate the photon energies (and k_z values) for the spin measurements.

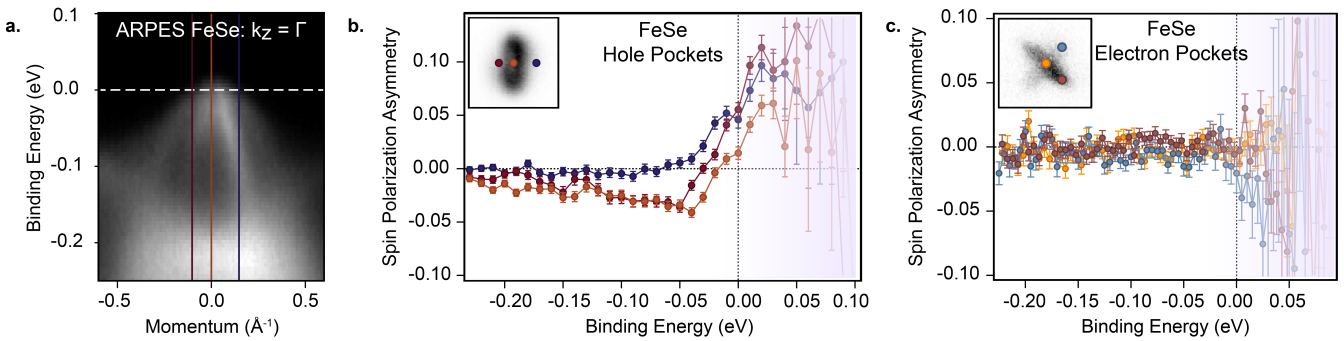

Figure 4 (a) ARPES near normal emission for orthorhombic FeSe at $h\nu = 37$ eV (k_z = Γ). Vertical lines indicate the direction for spin-resolved measurements. (b) Out of plane Spin Polarization Asymmetry (P_z) for normal emission, with inset showing cursors on the FeSe Fermi surface. Inset indicates the relevant momenta points on the Fermi surface. From this we see that sample is largely detwinned, with intensity primarily from one domain. (c) Same as (b) for the electron pockets of FeSe shows no observable P_z, suggesting an unobservably small coupling of $\vec{L}$ and $\vec{S}$ on the electron pockets. Non-zero contribution from twin domains allows for probing of both X and Y points. Curves correspond to the X/Y point (yellow), on the edge of the X pocket (red) and the Y pocket (blue).

Methods

FeSe crystals were grown via vapour transport technique[19] and LiFeAs by a self-flux method[23]. Samples were cleaved and measured in the non-superconducting phase at 20 K at pressure of 10^{-10} mbar at the APE-LE endstation at ELETTRA using a Scienta DA30 analyzer equipped with a VLEED-based spin-detector[14]. The electronic structure has been calculated using the QUANTUM ESPRESSO[24] package, and the output post-processed using Wannier90[25], projecting the low-energy electronic states near E_F onto a reduced basis of maximally localized wavefunctions of Fe 3d and As 4p character. A pseudo $ab\ initio$ tight-binding Hamiltonian based on the Wannier90 Hamiltonian was used for calculations of ARPES intensity and $\left\langle \vec{L} \cdot \vec{S} \right\rangle$. Atomic spin orbit coupling was added to Fe orbitals as a parameter.

1. Hirschfeld, P. J., Korshunov, M. M. & Mazin, I. I. Gap Symmetry and Structure of Fe-Based Superconductors. *Reports on Progress in Physics* **74**, 124508 (2011). URL `http://stacks.iop.org/0034-4885/74/i=12/a=124508`.

2. Hirschfeld, P. J. Using Gap Symmetry and Structure to Reveal the Pairing Mechanism in Fe-Based Superconductors. *Comptes Rendus Physique* **17**, 197 – 231 (2016). URL `http://www.sciencedirect.com/science/article/pii/S1631070515001693`. Iron-based superconductors / Supraconducteurs base de fer.

3. Fernandes, R. M. & Chubukov, A. V. Low-Energy Microscopic Models for Iron-Based Superconductors: A Review. *Reports on Progress in Physics* **80**, 014503 (2017). URL `http://stacks.iop.org/0034-4885/80/i=1/a=014503`.

4. van Roekeghem, A., Richard, P., Ding, H. & Biermann, S. Spectral Properties of Transition Metal Pnictides and Chalcogenides: Angle-Resolved Photoemission Spectroscopy and Dynamical Mean-Field Theory. *Comptes Rendus Physique* **17**, 140 – 163 (2016). URL http://www.sciencedirect.com/science/article/pii/S1631070515002200. Iron-based superconductors / Supraconducteurs base de fer.

5. Brouet, V. *et al.* Impact of the Two Fe Unit Cell on the Electronic Structure Measured by ARPES in Iron Pnictides. *Phys. Rev. B* **86**, 075123 (2012). URL https://link.aps.org/doi/10.1103/PhysRevB.86.075123.

6. Borisenko, S. V. *et al.* Direct Observation of Spin-Orbit Coupling in Iron-Based Superconductors. *Nat Phys* **12**, 311–317 (2016). URL http://dx.doi.org/10.1038/nphys3594.

7. Fernandes, R. M. & Vafek, O. Distinguishing Spin-Orbit Coupling and Nematic Order in the Electronic Spectrum of Iron-Based Superconductors. *Phys. Rev. B* **90**, 214514 (2014). URL https://link.aps.org/doi/10.1103/PhysRevB.90.214514.

8. Zhu, Z.-H. *et al.* Layer-By-Layer Entangled Spin-Orbital Texture of the Topological Surface State in Bi_2Se_3. *Phys. Rev. Lett.* **110**, 216401 (2013). URL https://link.aps.org/doi/10.1103/PhysRevLett.110.216401.

9. Liu, Y. Visualizing Electronic Chirality and Berry Phases in Graphene Systems Using Photoemission with Circularly Polarized Light. *Physical Review Letters* **107** (2011).

10. Veenstra, C. N. *et al.* Spin-Orbital Entanglement and the Breakdown of Singlets and Triplets in Sr_2RuO_4 Revealed by Spin- and Angle-Resolved Photoemission Spectroscopy. *Phys. Rev. Lett.* **112**, 127002 (2014). URL https://link.aps.org/doi/10.1103/PhysRevLett.112.127002.

11. Mizokawa, T. *et al.* Spin-Orbit Coupling in the Mott Insulator Ca_2RuO_4. *Phys. Rev. Lett.* **87**, 077202 (2001). URL https://link.aps.org/doi/10.1103/PhysRevLett.87.077202.

12. Pierce, D. T. & Meier, F. Photoemission of Spin-Polarized Electrons from GaAs. *Phys. Rev. B* **13**, 5484–5500 (1976). URL https://link.aps.org/doi/10.1103/PhysRevB.13.5484.

13. While this is only strictly true for normal incident light, these selection rules are largely preserved, even for light incident as in our experiment at 45^o. See Supplementary Materials Figure S2.

14. Bigi, C. *et al.* Very Efficient Spin Polarization Analysis (VESPA): New Exchange Scattering-Based Setup for Spin-Resolved ARPES at APE-NFFA Beamline at Elettra. *Journal of Synchrotron Radiation* **24**, 750–756 (2017).

15. Ferber, J., Foyevtsova, K., Valentí, R. & Jeschke, H. O. LDA + DMFT Study of the Effects of Correlation in LiFeAs. *Phys. Rev. B* **85**, 094505 (2012). URL https://link.aps.org/doi/10.1103/PhysRevB.85.094505.

16. Saito, T., Yamakawa, Y., Onari, S. & Kontani, H. Revisiting Orbital-Fluctuation-Mediated Superconductivity in LiFeAs: Nontrivial Spin-Orbit Interaction Effects on the Band Structure and Superconducting Gap Function. *Phys. Rev. B* **92**, 134522 (2015). URL https://link.aps.org/doi/10.1103/PhysRevB.92.134522.

17. Damascelli, A. Probing the Electronic Structure of Complex Systems by ARPES. *Physica Scripta* **2004**, 61 (2004). URL http://stacks.iop.org/1402-4896/2004/i=T109/a=005.

18. Fernandes, R. M., Chubukov, A. V. & Schmalian, J. What Drives Nematic Order in Iron-Based Superconductors? *Nat Phys* **10**, 97–104 (2014). URL http://dx.doi.org/10.1038/nphys2877.

19. Böhmer, A. E. *et al.* Lack of Coupling Between Superconductivity and Orthorhombic Distortion in Stoichiometric Single-Crystalline FeSe. *Phys. Rev. B* **87**, 180505 (2013). URL https://link.aps.org/doi/10.1103/PhysRevB.87.180505.

20. Watson, M. D. *et al.* Emergence of the Nematic Electronic State in FeSe. *Phys. Rev. B* **91**, 155106 (2015). URL https://link.aps.org/doi/10.1103/PhysRevB.91.155106.

21. Cvetkovic, V. & Vafek, O. Space Group Symmetry, Spin-Orbit Coupling, and the Low-Energy Effective Hamiltonian for Iron-Based Superconductors. *Phys. Rev. B* **88**, 134510 (2013). URL https://link.aps.org/doi/10.1103/PhysRevB.88.134510.

22. Vafek, O. & Chubukov, A. V. Hund Interaction, Spin-Orbit Coupling, and the Mechanism of Superconductivity in Strongly Hole-Doped Iron Pnictides. *Phys. Rev. Lett.* **118**, 087003 (2017). URL https://link.aps.org/doi/10.1103/PhysRevLett.118.087003.

23. Chi, S. *et al.* Scanning Tunneling Spectroscopy of Superconducting LiFeAs Single Crystals: Evidence for Two Nodeless Energy Gaps and Coupling to a Bosonic Mode. *Phys. Rev. Lett.* **109**, 087002 (2012). URL https://link.aps.org/doi/10.1103/PhysRevLett.109.087002.

24. Giannozzi, P. *et al.* Quantum espresso: a modular and open-source software project for quantum simulations of materials. *Journal of Physics: Condensed Matter* **21**, 395502 (19pp) (2009). URL http://www.quantum-espresso.org.

25. Mostofi, A. A. *et al.* An Updated Version of Wannier90: A Tool for Obtaining Maximally-Localised Wannier Functions. *Computer Physics Communications* **185**, 2309 – 2310 (2014). URL http://www.sciencedirect.com/science/article/pii/S001046551400157X.